



Evaluation of the IGS-Global Ionospheric Mapping model over Egypt 1

Mostafa RABAH¹, Ahmed Sedeek² 2

¹: Civil Eng. Dpt., Benha Faculty of Engineering, Benha University, Egypt., 3

*Correspondence: mrabah@bhit.bu.edu.eg 4

²: Civil Eng. Dept., Higher Institute of Engineering and Technology - Bihira, Egypt 5

Abstract: 6

Global ionosphere maps (GIM) are generated on a daily basis at CODE using data from about 400 7
GPS/GLONASS sites of the IGS and other institutions. The vertical total electron content (VTEC) is 8
modeled in a solar-geomagnetic reference frame using a Spherical Harmonics Expansion “SHE” up 9
to degree and order 15. To cover the holes of the first GIM computation stage existing in the North 10
Africa and over the Oceans resulting a shortage of GNSS station in North Africa, an optimum 11
spatial-temporal interpolation technique was developed to cover these holes (Krankowski and 12
Hernandez-Pajares, 2016). 13

The current paper evaluates the ionospheric correction by Global Ionospheric Maps, GIM, provided 14
in (IONEX) files produced by International GNSS Services “IGS”. The evaluation is performed 15
based on investigating the effect of a given GIM ionospheric correction on kinematic relative 16
positioning solutions. The evaluation was done using several baselines of different lengths in Egypt. 17
The results show that there is no significant effect of the provided GIM values on the solution of 18
kinematic processing. The results confirm that although there is a lack of International GNSS Service 19
(IGS stations) over North Africa, GIMs have no effect in mitigating ionospheric error. A new value 20
for the ionosphere correction VTEC values was obtained by a regional, developed algorithm based 21
on zero-differenced phase ionospheric delay (ZDPID) (Tawfeek et.al., 2018). These new values of 22
VTEC were fed into GIMs for the specified stations data. A useful result was obtained for correcting 23
the ionospheric error over kinematic solution of many baseline lengths up to 300 km which 24
demonstrates validity of the proposed evaluation method. 25

Key words: International GNSS Services “IGS”, Global ionospheric maps “GIM”, vertical total 26
electron content (VTEC), Zero-differenced phase ionospheric delay 27

1. Introduction 28

Global ionosphere maps (GIM) are generated on a daily basis at CODE using data from about 400 29
GPS/GLONASS sites of the IGS and other institutions, see figure (1). The vertical total electron 30



content (VTEC) is modeled in a solar-geomagnetic reference frame using a Spherical Harmonics Expansion “SHE” up to degree and order 15. Piece-wise linear functions are used for representation in the time domain. The time spacing of their vertices is 2 hours, conforming with the epochs of the VTEC maps. Instrument biases, so-called differential P1-P2 code biases (DCB), for all GPS satellites and ground stations are estimated as constant values for each day, simultaneously with the 3328 parameters used to represent the global VTEC distribution. The DCB datum is defined by a zero-mean condition imposed on the satellite bias estimates. P1-C1 bias corrections are taken into account if needed. To convert line-of-sight TEC into vertical TEC, a modified single-layer model (MSLM) mapping function approximating the JPL extended slab model mapping function is adopted. The global coverage of the GPS tracking ground stations considered at CODE is shown in figure (1).

According to Hernández-Pajares et al. (2017), broadly used Global Ionosphere Maps (GIMs) provided by the IGS are characterized by estimated accuracy ranging from a few TECU to approximately 10 TECU in VTEC. This IGS product offers 2.5 by 5.0 degrees spatial resolution, and temporal resolution of 2 h. IGS GIMs are developed as an official product of the IGS Ionosphere Working Group by performing a weighted mean of the various Analysis Centers (AC) VTEC maps: CODE, ESA, JPL, UPC, and NRCan. CODE GIM (CODG) comes from processing double-differenced carrier phase data and TEC parametrization using Spherical Harmonics Expansion “SHE” functions and Bernese software (Schaer, 1999). ESA GIM is based on processing carrier phase-smoothed pseudoranges and TEC parametrization using SHE functions (Feltens, 2003). JPL GIM is derived from a three-shell model that is based on spline functions.

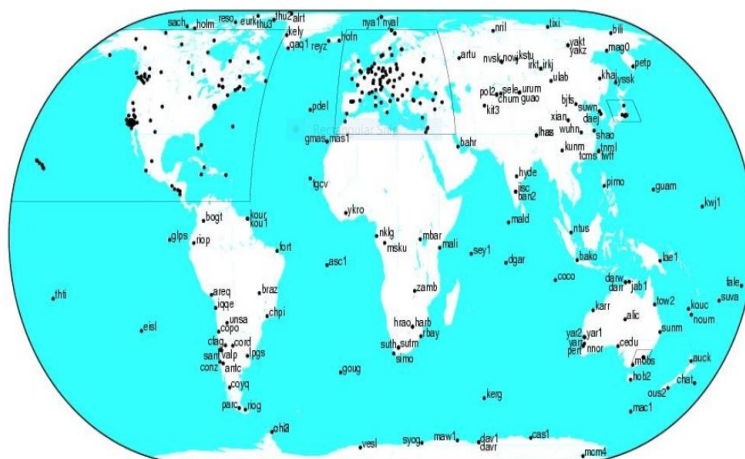




Figure (1): IGS directly manages ~400 permanent GNSS stations observing 4-12 satellites at 30 s 52
rate: more than 250,000 STEC observations/hour worldwide, but there is lack of stations in some 53
areas (e.g., over the oceans). 54

According to Hernández-Pajares et al. (2009), the highest accuracy is offered by the UQRG model 55
provided by UPC, and is produced by combining a tomographic modelling of the ionosphere with 56
kriging interpolation using the TOMION software developed at UPC. UQRG offers 2.5 by 5.0 57
degrees spatial resolution, and high temporal resolution of 15 min (Orús et al., 2005). It should also 58
be noted that vertical TEC values estimated by using smoothed pseudoranges have lower accuracy 59
than values offered by methods based on the precise carrier phase observations. 60

The majority of various global and regional ionosphere models currently available are characterized 61
by low temporal and spatial resolutions. Most of them are based on carrier phase-smoothed 62
pseudorange data, which presents low accuracy and requires strong smoothing filters. As a result, the 63
obtained ionospheric delay represents relatively low accuracy of several TEC units (1 Total Electron 64
Content Unit = 1 TECU = 10^{16} el/m², and it is equivalent to 0.162 m of L1 signal delay). This is one 65
of the reasons why spherical harmonics expansion (SHE) is used for the global and regional TEC 66
parameterization (Rovira-Garcia, 2017). The smoothing effect of SHE undoubtedly results in the low 67
accuracy of the ionospheric models. Also, the ionosphere models often use GPS-only data. Another 68
important aspect is using a single layer model (SLM) ionosphere approximation and its associated 69
relatively simple mapping function, which results in a rather low relative accuracy of publically 70
available models that amounts to 20–30%, as was shown in Hernández-Pajares et al. (2011). 71

Precise kinematic positioning to centimeter level accuracy requires using the carrier phase 72
observations with the correct resolution of the integer ambiguities. Conclusions previously published 73
for solving the ambiguities of medium baselines On-The-Fly can be summarized in the following 74
two different approaches (El-Hattab et al., 2003): 75

1. The main layout of the first approach can be represented by the following two steps: The first 76
step is a static initialization for the rover receiver at the beginning of the mission within a short 77
distance with respect to a reference receiver. This will facilitate the processing of the ambiguity 78
fixing. In the second step, a technique for ambiguity recovery On-The-Fly is introduced to 79
recover the integer ambiguities when cycle slips or data gaps shorter than a few minutes occur. 80
2. The second approach mainly depends on the condition that the dominant source of distance- 81
dependent errors is the ionospheric refraction compared to the orbit error as well as the 82
tropospheric error. As is known, the tropospheric error is mostly affected by the height difference 83



between the ends of the baseline rather than the distance. Hence, the ionospheric error produces 84
 the dominant contribution in complicating the ambiguity resolution of a medium baseline 85
 compared to the other errors. Therefore, providing a proven correct ionospheric correction to the 86
 processing will enhance the ambiguity resolution process. 87

The current study evaluates the possibility of using Global Ionospheric Maps for mitigating 88
 ionosphere effect (large error source) over Egypt. The evaluation process is undertaken by 89
 incorporating the derived GIM-VTEC values into the processing of baselines different lengths (up to 90
 300 km) in kinematic mode to check how the processing results are improved. Finally, the analysis 91
 of the obtained results and graphs supported with the statistical analysis is discussed and presented, 92
 from which the important conclusions and recommendations are drawn. 93

2 Methodology 94

2.1 GPS Observation equations 95

The observation equations for code and carrier phase measurements on the L_i frequency ($i = 1, 2$) can 96
 be formulated as follows (Hoffmann et al., 2013): 97

$$P(L_i) = \rho + c(dt - dT) + d_{orb} + d_{trop} + d_{ion/li} + d_{mult(P_{li})} + \epsilon(P_{li}) \quad (1) \quad 98$$

$$\varphi(L_i) = \rho + c(dt - dT) + d_{orb} + d_{trop} + d_{ion/li} + \lambda_i N_i + \lambda_i(\varphi_r(to, li) - \varphi_s(to, li)) + d_{mult(\varphi_{li})} + \epsilon(\varphi_{li}) \quad (2) \quad 99$$

Where: 100

$P(L_i)$: Measured pseudo range on Li (m).	101
$\varphi(L_i)$: Measured carrier phase on Li (m).	102
ρ	: True geometric range (m).	103
c	: Speed of light (m/s).	104
dt	: Satellite clock error (s).	105
dT	: Receiver clock error (s).	106
d_{orb}	: Satellite orbital error (m).	107
d_{trop}	: Tropospheric delay (m).	108
$d_{ion/li}$: Ionospheric delay on Li (m).	109
λ_i	: Wavelength (m).	110
N_i	: Integer ambiguity on Li (cycle).	111
		112



$\varphi_r(to, li)$: Initial phase of receiver oscillator.	113
$\varphi_s(to, li)$: Initial phase of satellite oscillator.	114
$d_{mult}(P_{ii})$: Multipath effect in measured pseudo range on Li (m).	115
$d_{mult}(\varphi_{ii})$: Multipath effect in measured carrier phase on Li (m).	116
$\epsilon(P_{ii})$: Measurement noise (m).	117

Denoting the stations by a and b and the satellites involved by j, k, the double difference model for long baselines when there is a significant difference in the atmospheric effect between the two baselines ends and elevation angles at both stations are different can be expressed:

$$\begin{aligned} \nabla\Delta\varphi_{ab}^{jk}(t) = & \rho_a^j(t) - \rho_a^k(t) - \rho_b^j(t) + \rho_b^k(t) + \lambda\nabla\Delta N_{ab}^{jk}(t) + \nabla\Delta dorb_{ab}^{jk}(t) + \nabla\Delta dtr\text{op}_{ab}^{jk}(t) \\ & - \nabla\Delta dion_{ab}^{jk}(t) + \nabla\Delta dmult_{ab}^{jk}(t) + \nabla\Delta\epsilon_{ab}^{jk}(t) \end{aligned} \quad (3)$$

The term $\nabla\Delta N_{ab}^{jk}(t)$ is called the double difference integer ambiguity, that must be determined (as an integer) during the double difference carrier phase processing procedure. If the individual carrier phase observations are continuously made over time (no cycle slip), the integer ambiguity terms remain constant. If these terms can be successfully determined to integer values, the fixed solution to the baseline is achievable. In the case of short base lines, the residual orbital errors ($\nabla\Delta dorb_{ab}^{jk}(t)$), residual ionospheric errors ($\nabla\Delta dion_{ab}^{jk}(t)$), and residual tropospheric errors ($\nabla\Delta dtr\text{op}_{ab}^{jk}(t)$) can be considered negligible (Hofmann, 2008). Multipath errors are not mitigated by differencing observations, and hence a user should try to avoid multipath environments whenever possible as the best approach to mitigating their effects (Abu Galala et al., 2018).

For medium and long baselines common error does not cancelled out. Because of different elevation angles on both ends of baseline there is no correlation between the errors. Using precise orbit and clock products with centimeter level accuracy, the two errors related with the broadcast orbits and clocks can be significantly reduced. Satellite and receiver clock error does not depend on baseline length, so it can be cancelled by differencing. For the tropospheric residual errors, the best standard method of computing is to apply a tropospheric error model at the locations of the reference and remote stations. Examples of such models include the Hopfield model and the Saastamoinen model (Hoffman, 2008).

2.2 Ionospheric modelling



The ionospheric delay has an intensive impact on the GNSS observations by driving an additional transmission time delay. The magnitude of this effect is determined by the amount of total electron content (TEC) and the frequency of signal. Under normal solar activity conditions, this effect on GPS signals is usually in the range from a few meters to tens of meters, but it can reach more than 100 m during severe ionosphere storms (Rovira-Garcia, 2015). TEC is quantified from GPS measurements by a linear combination of the measured pseudo range and phase observables registered by the receiver on two carrier frequencies ($f_1 = 1575.4$ MHz and $f_2 = 1227.6$ MHz). TEC is measured in TECU units with $1 \text{ TECU} = 10^{16} \text{ el/m}^2$.

The geometry-free linear combination of GPS observations is used for ionospheric estimation and it is obtained by subtracting simultaneous pseudo range ($P_1 - P_2$ or $C_1 - P_2$) or carrier phase observations ($\varphi_1 - \varphi_2$). Code-based TEC (TEC_P) is noisier than phase-based TEC (TEC_φ), largely due to multipath, but the phase-based suffers an unknown integer ambiguity offset and is subject to cycle slips associated with rapid ionospheric scintillations. The resultant TEC is the GPS-derived slant TEC along the signal path between satellite and receiver (Zus et al., 2017). In this combination, the satellite – receiver geometrical range and all frequency independent biases are removed. The geometry-free linear combination for carrier phase observations is obtained:

$$L_4(t) = \varphi_{CF} = \varphi_1 - \varphi_2 = (\gamma - 1)dion_1 + \lambda_1 N_1 - \lambda_2 N_2 + \varepsilon(\varphi_1 - \varphi_2) \quad (4)$$

Where: $\varepsilon(\varphi_1 - \varphi_2)$ is the noise term in phase equation can be neglected for simplicity, the factor γ is the factor to convert the ionospheric delay from L2 to L1 frequency.

$$dion_2 = \frac{40.3 \text{ STEC}}{f_2^2} = \frac{f_1^2}{f_2^2} Dion_1 = \gamma Dion_1 \quad \gamma = \frac{f_1^2}{f_2^2} \quad (5)$$

2.3 VTEC Estimation

The ionosphere may be considered as a thin single layer surrounding the earth at a fixed height from the earth for which all free electrons in the ionosphere are assumed to be concentrated, in this single-layer having a maximum electron density (10^{11} : 10^{12} e/m^2 around 300-500 km) (Feltens, 2003). IPP is the intersection point between the satellite receiver line-of-sight, and the ionosphere shell (Figure 2). Slant total electron content (STEC) can be translated into VTEC using Single Layer Model (SLM).

$$VTEC = F(E) \text{ STEC}$$



$$VTEC = F(E) \frac{dion_1 \cdot f_1^2}{40.3}$$

Where: $F(E)$ is the mapping function.

Mapping function model:

To compute elevation and azimuth angle for any satellite, the satellite position coordinate (x_s, y_s, z_s) in ECEF at the specified epoch is deduced from the IGS final orbits. The interpolated satellite position is then transformed to a local coordinate frame, East, North, and Up (ENU) system. The transferred ENU is used to calculate elevation and azimuth angles as follows (Sedeek et al., 2017):

$$E = \arctan\left(\frac{x_U}{\sqrt{x_N^2 + x_E^2}}\right) \quad A = \arctan\left(\frac{x_E}{x_N}\right)$$

Where: E and A are elevation angle and Azimuth angle of satellite at the receiver, respectively. The receiver position in Earth Centered Earth Fixed (ECEF) is converted to geodetic coordinates. Ionospheric Pierce Point (IPP) is the intersection point between the satellite and the receiver line-of-sight. Ionospheric Pierce Point (IPP) location can be computed by providing reference station coordinates (ϕ_r, λ_r) , from which the geographic latitude and longitude of IPP can be computed according to elevation and azimuth angle of satellite as follows (Sedeek et al., 2017):

$$\psi = \pi / 2 - E' - E$$

Where ψ : The offset between the IPP and the receiver; E' and E : the elevation angles of the satellite at the IPP and receiver.

$$E' = \sin^{-1}\left(\left(\frac{R_E}{R_E + H}\right) \cos E\right)$$

R_E : is the mean radius of the spherical Earth (6371 km)

H : is the height of IPP (taken to be 450 km)

$$\phi_{IPP} = \sin^{-1}(\sin(\phi_r) \cdot \cos(\psi) + \cos(\phi_r) \cdot \sin(\psi) \cdot \cos(A))$$

$$\lambda_{IPP} = \lambda_r + \frac{\psi \cdot \sin(A)}{\cos(\phi_{IPP})}$$

169

170

171

172

173

174

175

176

177

178

179

180

181

182

183

184

185

186

187

188

189

190

191

192

193

194



3. GIM Evaluation

To evaluate the obtained ionospheric TEC values that are produced by IGS, the IONEX data file for a specified time is imported. This data if used with GNSS data should improve the position solution and/or enhance ambiguity resolution of a specified baseline that cannot be fixed under normal conditions, otherwise the quality of the imported ionospheric data is not good enough to support the positioning works. However, our evaluation approach is built on applying the imported IONEX data on a third-party processing SW, Trimble Total Control, known as TTC, for collected baselines of different lengths. The processing is performed on a kinematic mode. Alternative ion TEC data, generated by regional model was applied to evaluate the validity of the proposed evaluation approach.

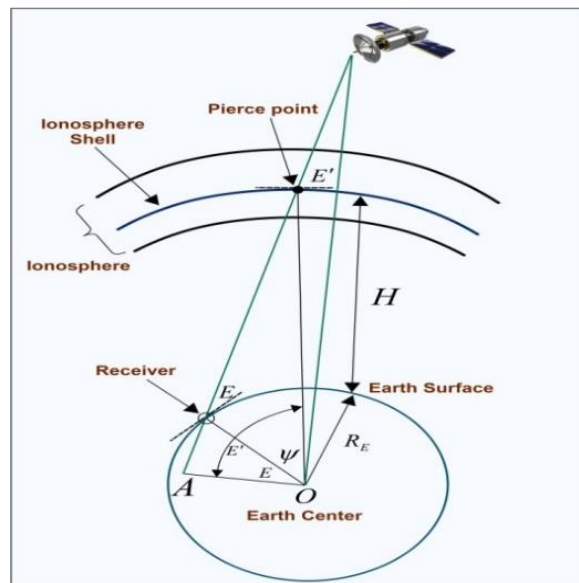


Figure (2): Elements of the spherical ionospheric shell model (Sedeek et al., 2017).

3.1 Data Description

The data used for the evaluation study, refer to figure (3), were collected on April 15, 2015 at seven stations: six of them, is the northern part of the Egyptian Permanent GNSS Network (EPGN) established by the National Research Institute of Astronomy and Geophysics NRIAG at 2006 and the seventh station in Alexandria managed by the French institute, Centre d'Études Alexandrines (CEALX). All NRIAG Stations are equipped with Trimble Net R5 Dual frequency GNSS receivers whilst Alexandria is equipped with a LEICA GRX1200 GG-Pro Dual frequency GNSS Receiver.



The data sample rate was 30 seconds epoch interval. The number of visible satellites varied between 224
6 and 10 during the test period. As is shown in figure (3), all the used GNSS stations are located 225
between Latitudes 30° & 32° and Longitudes 25° & 33° . 226

3.2 Processing Software 227

For baseline processing, Trimble Total Control 2.7 (TTC2.7) was the main processing software 228
package that was used for the kinematic processing of the data. TTC has the capability to implement 229
precise ephemeris and global ionospheric maps (IONEX). On the other hand, for Precise Point 230
Positioning (PPP), the online service provided by Natural Resources Canada (NRCan) was utilized to 231
provide the threshold values for comparison (Rabah et al., (2016). The **NRCan Online Precise Point** 232
Positioning Software is developed by NRCan to supply various users' application requirements. The 233
PPP service can be used to process data collected by any single-or dual-frequency receiver, and the 234
data can be observed in static or kinematic modes. PPP is accessible via the Internet by logging into 235
the NRCan website (http://www.geod.nrcan.gc.ca/online_data_e.php). 236

3.3 GIM data 237

Table (1) shows a part of the IONEX data that was assigned for the specified latitude location of first 238
epoch of day April 15, 2015. The evaluation process is **carried** out by incorporating the derived GIM- 239
VTEC values into the processing of different baseline lengths (up to 300 km), in kinematic mode and 240
check how the processing results are improved. The evaluation was performed on several lengths of 241
baselines, see table (2), and processed with TTC software, with and without IONEX in Kinematic 242
mode. Unfortunately, the results show that the IONEX file did not affect the results at all: no 243
differences were found in solutions with and without IONEX. The results confirm that there is no 244
significant effect of the provided GIM values on the solution of kinematic processing. The results of 245
GIM values forced us to check the validity of Ion TEC values in the IONEX file for the specified 246
area. A trial was undertaken to compute alternative regional TEC values using another model. 247
248
249

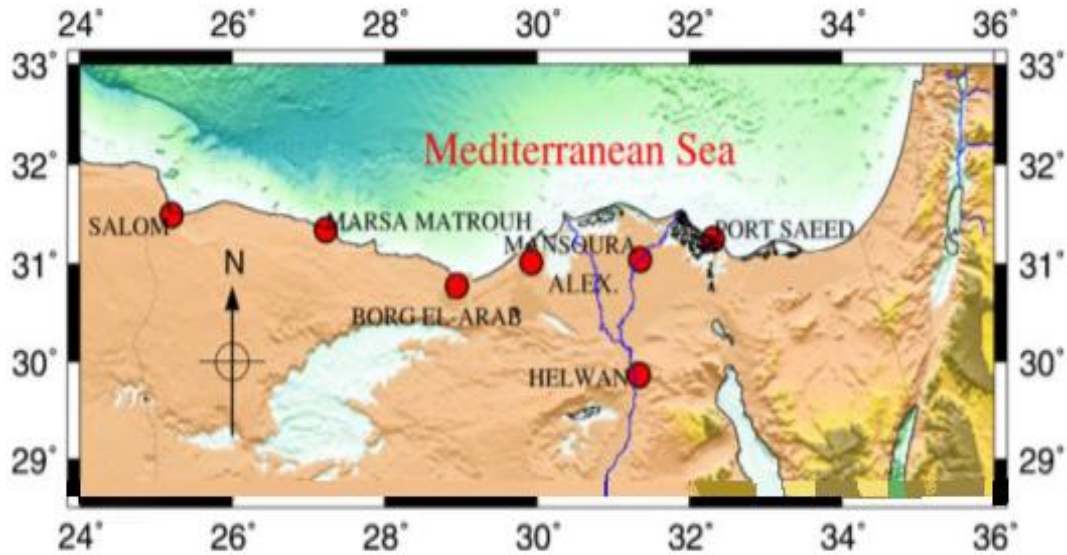


Figure (3): The location of the used stations

250
 251
 252
 253
 254

Table (1): Sample of the used IONEX file

2015	4	15	0	0	0	EPOCH OF CURRENT MAP									
32.5-180.0	180.0	5.0	450.0	LAT/LON1/LON2/DLON/H											
621	632	633	630	628	630	630	621	594	553	508	471	448	438	436	434
433	429	422	414	404	390	372	351	331	318	315	320	333	348	360	363
352	330	305	283	263	247	230	215	208	209	215	221	221	215	202	186
170	156	149	153	169	196	228	253	269	277	287	301	319	337	352	364
373	384	404	435	475	521	564	598	621							
30.0-180.0	180.0	5.0	450.0	LAT/LON1/LON2/DLON/H											
657	668	669	664	660	659	657	648	623	585	542	507	485	474	469	466
461	456	449	439	424	404	378	351	330	321	328	347	376	406	430	438
425	396	361	330	304	280	256	233	218	213	216	220	221	214	202	187
173	161	154	158	174	201	231	256	270	277	285	300	320	341	360	374
385	397	419	453	497	546	593	631	657							

255
 256

Table (2): The baseline used in verification

Baseline		
From	To	Length (Km)
Borg-Alarab (Borg)	Alexandria (Alex)	49.05
Port-Said (Said)	Mansura (Mnsr)	94.47
Helwan	Mansura (Mnsr)	130.76
Borg-Alarab (Borg)	Mansura (Mnsr)	171.11



Helwan	Port-Said (Said)	179.51
Helwan	Borg-Alarab (Borg)	203.05
Port-Said (Said)	Alexandria (Alex)	229.05
Borg-Alarab (Borg)	Port-Said (Said)	264.98

A new algorithm based on Zero-differenced phase Ionospheric Delay (ZDPID) was developed (Tawfeek et.al., 2018). The core of this algorithm is mainly dependant on computing the TEC values by using carrier phase and GPS phase ambiguity resolution model by using Sequential Least Square Adjustment. The proposed algorithm has been written using MATLAB code. The TEC values are computed for the aforementioned stations every epoch, 30 sec., then an average TEC values were computed every two hours similar to the GIM in IONEX file. The TEC values of the ZDPID with IONEX-IGS are depicted in figure (4). As is shown in figure (4), the TEC differences between the regional ZDPID values and the IONEX-IGS values exceed several tens of TEC units especially in the early morning with reduced values given at noon.

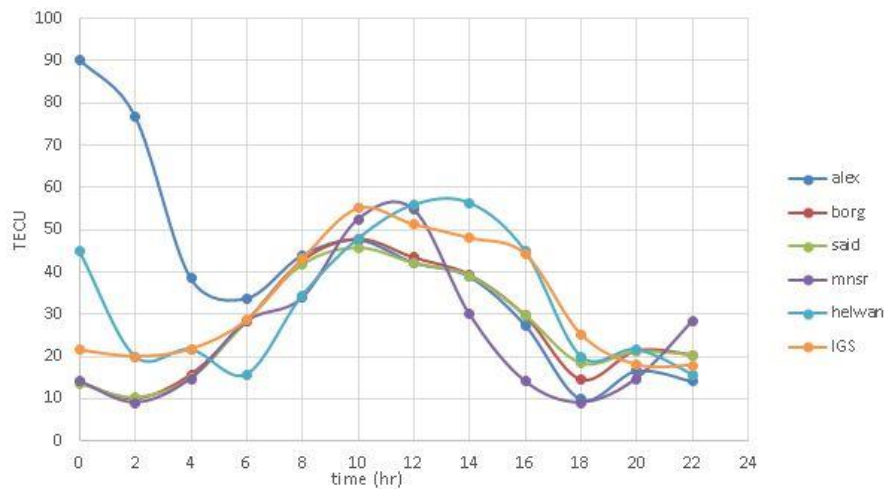


Figure (4): Mean TEC results every 2 hours of the study stations with comparison to IGS GIMs Day 105, 2015

Krankowski and Hernandez-Pajares (2016) confirmed that due to the shortage of GNSS stations in North Africa, the first GIM computation stage suffered from the hole existing in North Africa and over the Oceans, see figure (5). They deployed an optimum spatial-temporal interpolation technique to cover these holes. Based upon the above discussion, it is easy to confirm that the derived



ionospheric TEC values derived from IONEX GIM products are not feasible and useless for use in 274
precise positioning. 275

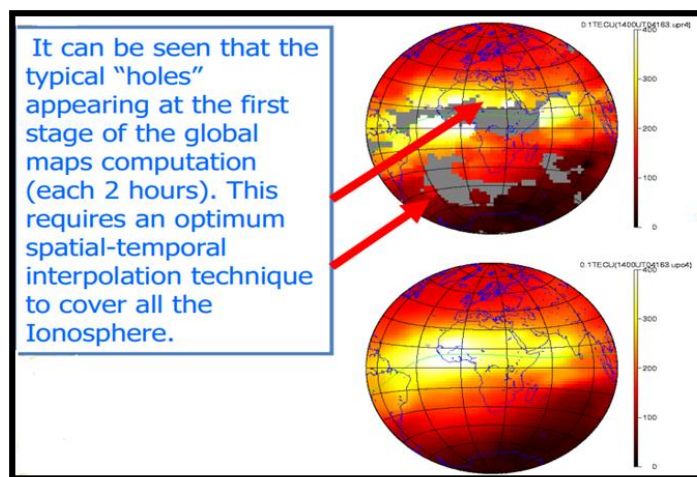


Figure (5): The holes of the GIM computation as indicated by (Krankowski and Hernandez-Pajares, 2016)

276
277
278
279
280
281
282
283
284
285
286
287
288
289
290
291
292
293
294
295
296
297

3.4 Modifying GIM-IONEX data

To modify the TEC data given in the IONEX file, the procedures described in the flow chart depicted in figure (6) were applied. Table (3) demonstrates a sample of the original TEC values as given in IONEX file and the modified values for Borg and Port Said stations at April 15, 2015. However, to see the validity of the computed regional Ionospheric TEC against the IONEX values, four baselines, namely Baseline Helwan ~ Mnsr 130.76 km, baseline Helwan ~ Said 179.51 km, baseline Helwan ~ Borg 203.16 km and baseline Borg ~ Said 264.98 km, were processed twice by TTC. The first processing was done without using any ionospheric correction and the second by using the modified IONEX files. The following chapter demonstrates the results of the processing of different baseline varying from 100 km to 270 km.

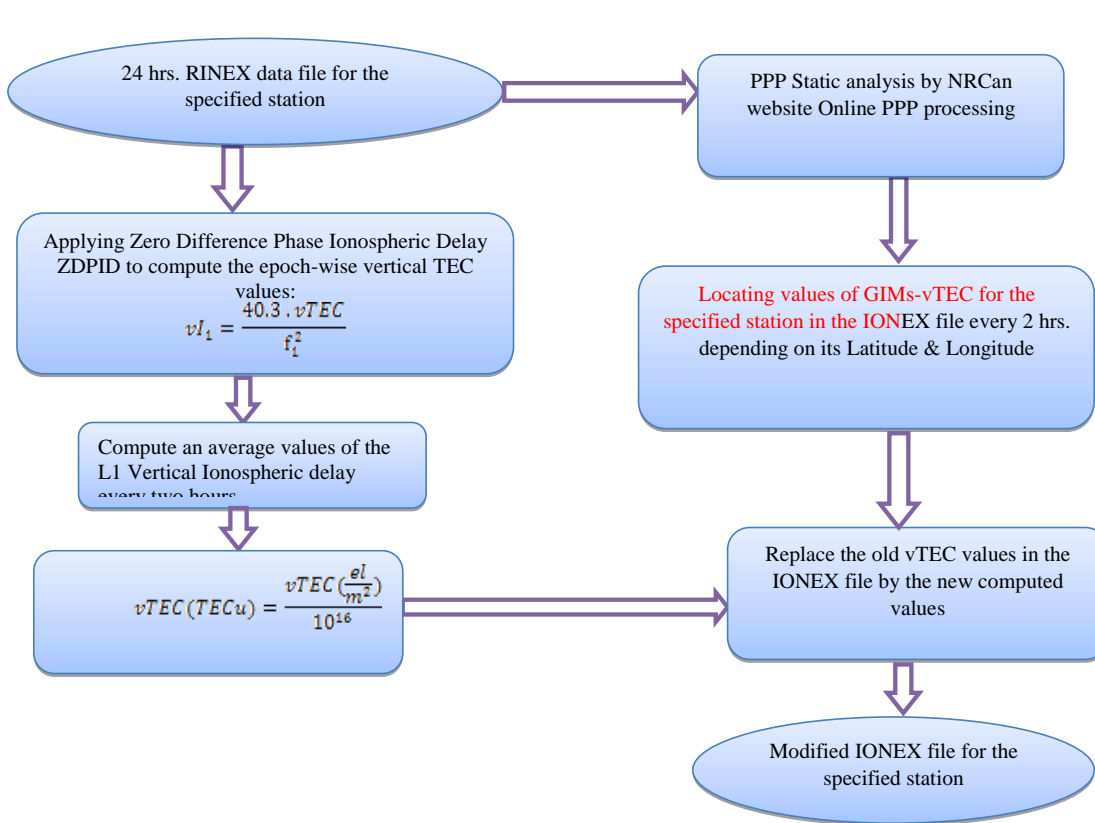


Figure (6): A description of the procedures that were used in modifying the VTEC values in the IONEX file.

Table (3): A sample Modified TEC values in IONEX file for the specified area in Egypt

32.5-180.0	180.0	5.0	450.0	LAT/LON1/LON2/DLON/H											
153	136	130	133	146	168	197	231	269	308	342	369	389	403	413	423
435	445	456	471	491	512	532	544	548	545	540	540	545	550	552	549
544	539	546	562	580	586	577	551	516	478	444	415	387	363	343	327
313	296	278	266	263	269	274	271	258	239	223	216	216	218	222	227
232	237	240	239	232	217	196	173	153							

The original TEC values given by IONEX at April15, 2015

298
 299
 300
 301
 302
 303
 304
 305
 306
 307
 308
 309
 310
 311
 312
 313
 314
 315
 316
 317
 318
 319
 320
 321
 322
 323
 324
 325
 326
 327
 328
 329
 330
 331



32.5-180.0	180.0	5.0	450.0	LAT/LON1/LON2/DLON/H											
153	136	130	133	146	168	197	231	269	308	342	369	389	403	413	423
435	445	456	471	491	512	532	544	548	545	540	540	545	550	552	549
544	539	546	562	580	586	577	551	516	478	141	415	387	363	343	327
313	296	278	266	263	269	274	271	258	239	223	216	216	218	222	227
232	237	240	239	232	217	196	173	153							
The TEC values given by ZDPID program at April15, 2015 for MNSR															
32.5-180.0	180.0	5.0	450.0	LAT/LON1/LON2/DLON/H											
153	136	130	133	146	168	197	231	269	308	342	369	389	403	413	423
435	445	456	471	491	512	532	544	548	545	540	540	545	550	552	549
544	539	546	562	580	586	577	551	516	478	298	415	387	363	343	327
313	296	278	266	263	269	274	271	258	239	223	216	216	218	222	227
232	237	240	239	232	217	196	173	153							
The TEC values given by ZDPID program at April15, 2015 for Port-Said Station															

4. Results and Discussion

The processing of the RINEX data was conducted using Trimble Total Control 2.7. The data were processed three times: the first run was performed by using the specified baselines data with normal default processing parameters, i.e. without using GIM. The second run was carried out using modified GIM and the third run was made using static precise point positioning for all 24-hours data of all stations to be used as a threshold reference values for comparison. The CSRS-PPP was deployed to give the required static solution for the specified stations, (Rabah et al., 2016). It should be borne that the two runs of TTC solutions were obtained without fixing the ambiguities i.e. float ambiguity solution. The TTC could not fix the ambiguities for the specified baselines. The discussion is therefore based on only how the Modified IONEX files provided with the TEC values computed by the ZDIPD algorithms improve the positioning.

The differences between the CRCS-PPP solution and the two TTC positioning solution were computed and are depicted in figures 7, 8, 9 & 10. Figures 7, 8, 9 and 10 show the position differences in easting, northing and ellipsoidal height between the computed static NRCAN PPP and the kinematic epoch by epoch solution in case of normal default processing parameters (D.D) and with using modified IONEX values (D.D.M-GIM). Figure (7) demonstrates how the modified IONEX, Mod-GIM, improve the kinematic solution of the baseline Borg-Mansura with length of

332

333

334

335

336

337

338

339

340

341

342

343

344

345

346

347

348

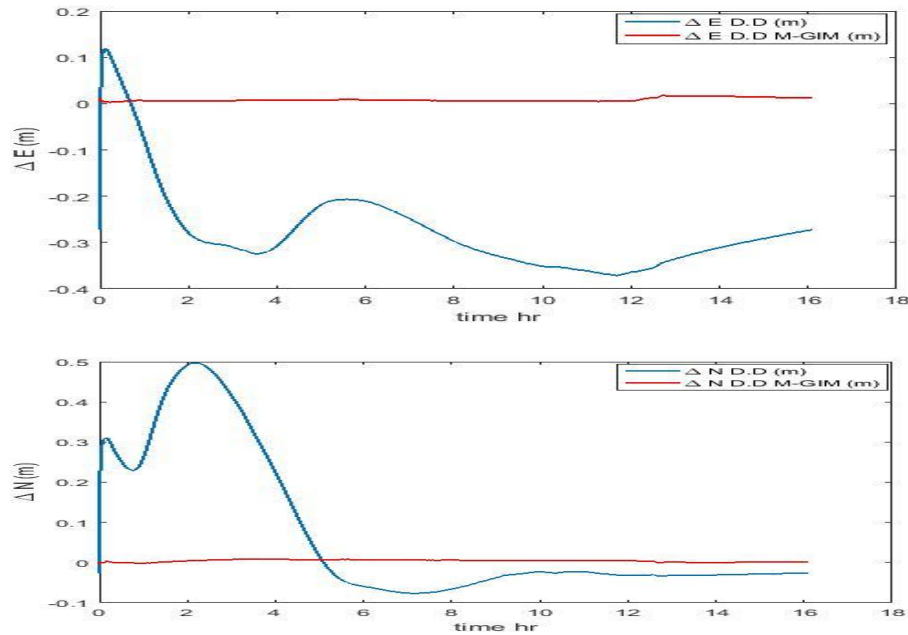
349

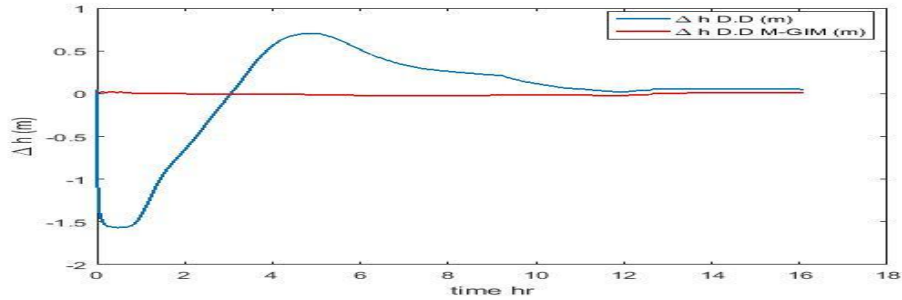
350

351



171.11 km. The differences between the two solutions were improved from (-37.11 & 11.89 cm) 352
with RMSE 29.07cm to (0.33& 1.79 cm) and RMSE of 0.93 cm for Easting component, and for the 353
northing component, the improvement ranged between the minimum value (-7.66 to -0.32 cm) and 354
the maximum values was reduced from (49.71 to 0.81cm), with the RMSE improved from (19.40 cm 355
to 0.5 cm). For the height components the differences were improved from (-156.74 & 70.55 cm) to 356
(-2.20 & 2.00cm) with an improvement the RMSE from 54.61cm to 1.43cm. 357
Figure (8) shows the effect of the modified Ion TEC value on improving the three components of 358
positioning of the baseline Helwan ~ Said of length 179.51 km. The figure depicts how the 359
Ionospheric value improve the quality and the quantity of the three positioning components. Figure 360
(9) demonstrates how the modified Ion TEC value improved the positioning solution of the Helwan ~ 361
Borg baselines of length 203.16 km. Finally, as it is seen in figure (10), the three components of 362
positioning of the baseline Borg ~ Said of length 264.98 km were improved. 363
364

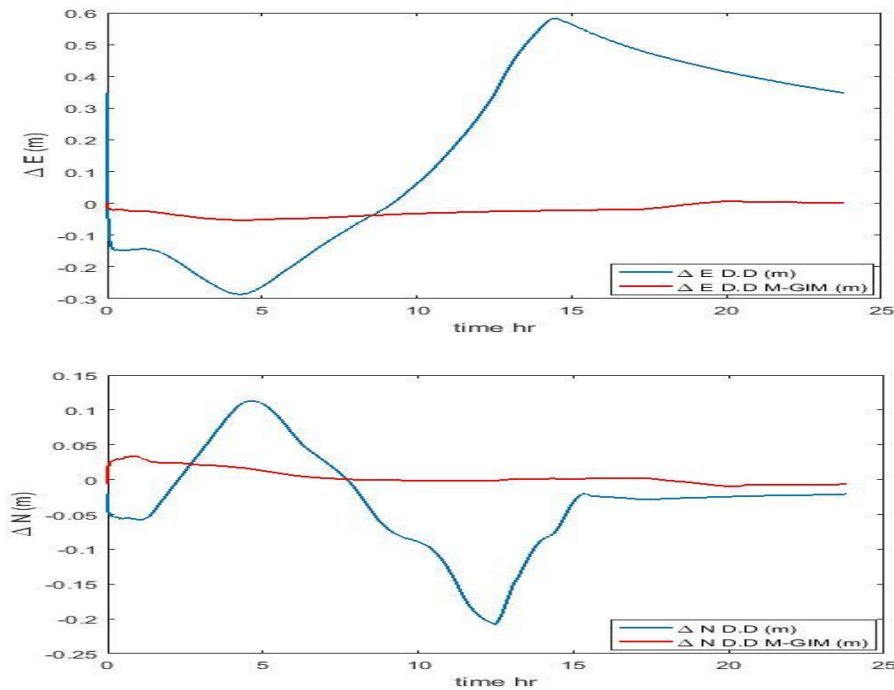


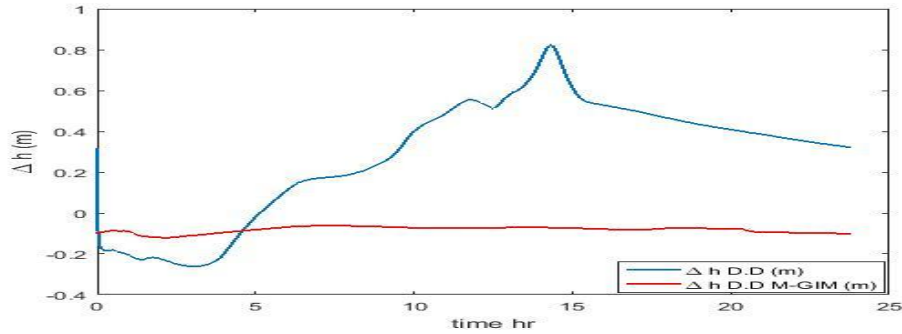


Statistical Item	Double Diff			Double Diff with Mod-IONEX		
	ΔE	ΔN	Δh	ΔE	ΔN	Δh
Min(cm)	-37.11	-7.66	-156.74	0.33	-0.32	-2.20
Max(cm)	11.89	49.71	70.55	1.79	0.81	2.00
Mean(cm)	-27.42	7.07	1.03	-0.84	0.42	-0.73
Rms(cm)	29.07	19.40	54.61	0.93	0.50	1.43

Figure (7): Positioning error with and without Mod. GIM in (East, North, Up) components between static PPP solution and relative kinematic positioning with Statistics for base line Borg~ Mnsr 171.11 km

365
 366
 367

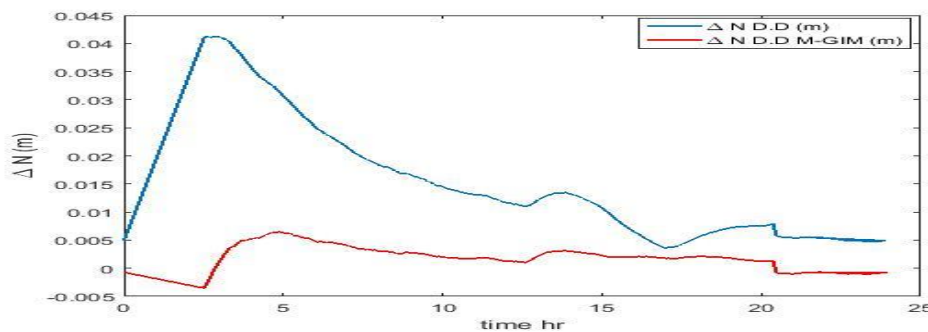
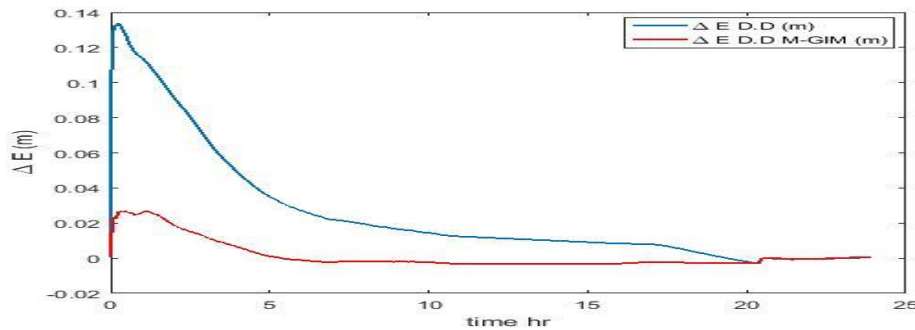


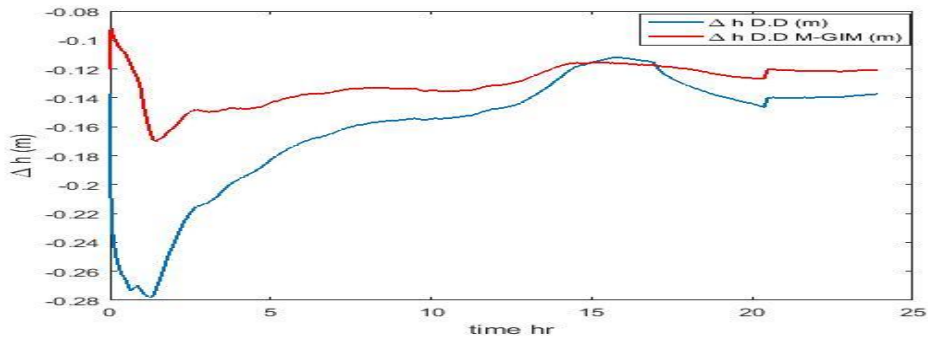


Statistical Item	Double Diff			Double Diff with Mod-IONEX		
	ΔE	ΔN	Δh	ΔE	ΔN	Δh
Min(cm)	-28.60	-20.80	-26.17	-5.26	-0.98	-12.10
Max(cm)	58.28	11.31	82.24	0.81	3.38	-6.25
Mean(cm)	17.00	-3.19	27.78	-2.42	0.38	-8.21
Rms(cm)	34.17	7.76	40.24	3.01	1.16	8.35

Figure (8): Positioning error with and without Mod-GIM in (East, North, Up) components between static PPP solution and relative kinematic positioning with Statistics for baseline Helwan ~ Said 179.51 km.

368
 369
 370

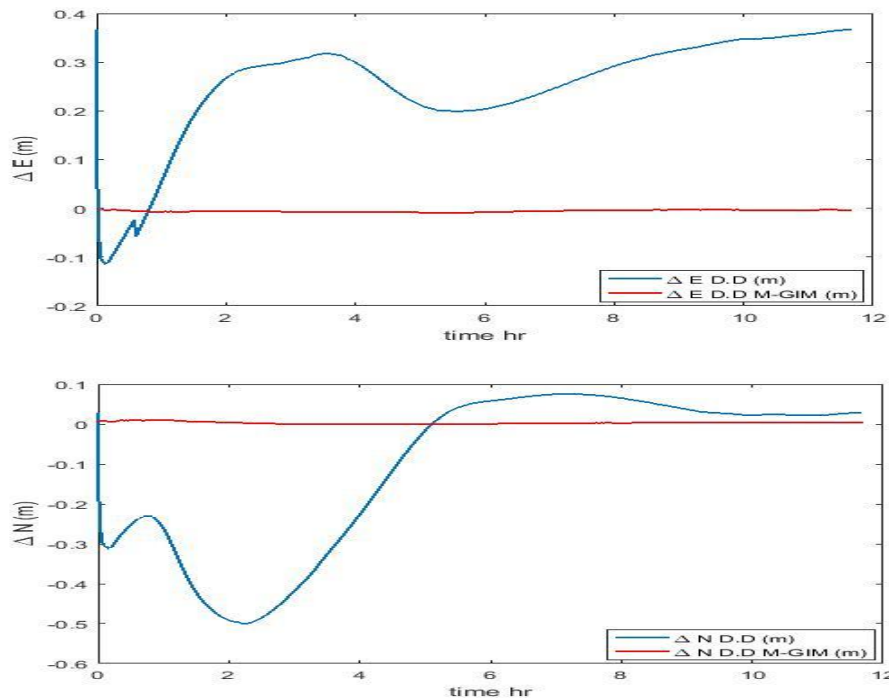


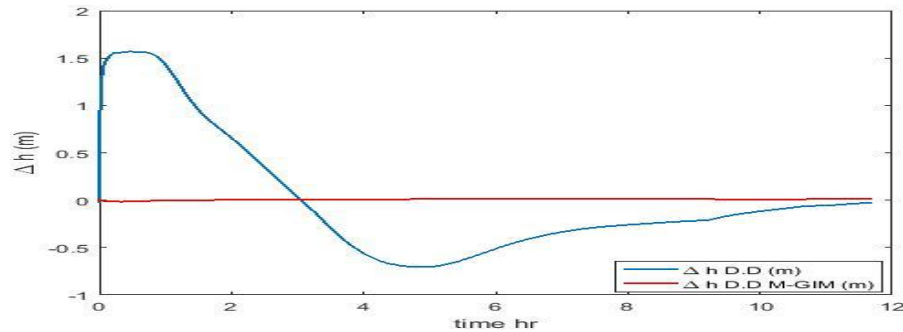


Statistical Item	Double Diff			Double Diff with Mod-IONEX		
	ΔE	ΔN	Δh	ΔE	ΔN	Δh
Min(cm)	-0.30	0.36	-27.80	-0.30	-0.36	-17.00
Max(cm)	13.37	4.13	-11.21	2.68	0.64	-9.21
Mean(cm)	2.90	1.36	-16.05	0.30	0.18	-13.02
Rms(cm)	4.65	1.70	16.55	0.92	0.27	13.08

Figure (9): Positioning errors with and without Mod-GIM in (East, North, Up) components between static PPP solution and relative kinematic positioning with Statistics for baseline Helwan ~ Borg 203.16 km.

371
 372
 373





Statistical Item	Double Diff			Double Diff with Mod-IONEX		
	ΔE	ΔN	Δh	ΔE	ΔN	Δh
Min(cm)	-11.36	-50.09	-70.55	-0.88	-0.04	-1.72
Max(cm)	36.74	7.54	156.79	0.20	1.04	1.86
Mean(cm)	25.07	-11.01	0.43	-0.56	0.32	0.84
Rms(cm)	27.32	22.77	64.04	0.59	0.42	1.13

Figure (10): Positioning error with and without Mod-GIM in (East, North, Up) components between static PPP solution and relative kinematic positioning with Statistics for baseline Borg ~ Said 264.98 km.

374
 375
 376
 377
 378
 379
 380
 381
 382
 383
 384
 385
 386
 387
 388
 389
 390
 391
 392
 393
 394
 395

5. Conclusions

The current paper evaluates the ionospheric correction by Global Ionospheric Maps, GIM, provided in (IONEX) files produced by International GNSS Services “IGS”. The evaluation is done based on investigating the effect of given GIM ionospheric correction on kinematic relative positioning solution. The evaluation has been performed on several baselines with different lengths in Egypt. Based upon the baselines processing results, the following conclusions can be drawn:

1. Due to the lack of GPS stations over the equatorial, North Africa and Atlantic in IGS network, the produced Global Ionospheric maps (GIMs) have poor effect for mitigating ionospheric error for precise positioning.
2. Evaluation of the TEC values in IONEX map by using estimated TEC values provided by Zero-differenced phase Ionospheric Delay (ZDPID) algorithm, a fruitful result is obtained for correcting ionospheric error over kinematic solution of many baseline lengths up to 265 km.
3. Most commercial software's such Leica Geo-Office, Trimble Total Control, Trimble Business Center failed to obtain accurate results for the kinematic solution of baseline lengths over 300 km.



6. References	396
Abou Galala M., M. Kaloop, M. Rabah, and Zaki Zidan: "Improving Precise Point Positioning Convergence Time through TEQC Multipath Observable". Paper Published in American Society of Civil Engineering, Journal of Surveying Engineering, J. Surv. Eng., 2018, 144(2): 04018002, 2018.	397 398 399
El-Hattab A. and M. Rabah : "Applying New Approaches for Improving the On-The-Fly (OTF) Ambiguity Resolution Process Over Long Baselines", Port Said Engineering Journal (PSERJ), Vol. 5 (2), September 2001, 334-345, 2001,	400 401 402
Feltens, J.: The International GPS Service (IGS) ionosphere working group. Adv. Space Res. 2003, 31, 205–214, 2003.	403 404
Hernández-Pajares, M., Juan, J.M., Sanz, J., Aragon-Angel, A., Garcia-Rigo, A., Salazar, D., Escudero, M.: "The ionosphere: Effects, GPS modeling and the benefits for space geodetic techniques". J. Geodesy 2011, 85, 887–907, 2011.	405 406 407
Hernandez-Pajares, M., Roma-Dollase, D., Krankowski, A., Garcia-Rigo, A., Orús-Perez, R.: Methodology and consistency of slant and vertical assessments for ionospheric electron content models. J. Geodesy 2017, 91, 1–10, 2017.	408 409 410
Hofmann-Wellenhof, B., H. Lichtenegger, and E. Wasle: "GNSS Global Navigation Satellite Systems; GPS, GLONASS, GALILEO & more". Springer Wien New York, 2008.	411 412
Krypiak-Gregorczyk, A., Wielgosz, P., Jarmołowski, W.: A new TEC interpolation method based on the least squares collocation for high accuracy regional ionospheric maps. Meas. Sci. Technol. 2017, 28, 045801, 2017.	413 414 415
Krankowski A. and M. Hernandez-Pajares: "LOFAR Ionospheric Workshop Space Research Centre of the Polish Academy of Science, 2016.	416 417
Komjathy, A., Schaer, S., Krankowski, A.: The IGS VTEC Maps: A Reliable Source of Ionospheric Information since 1998. J. Geodesy 2009, 83, 263–275, 2009.	418 419
Orús, R., Hernández-Pajares, M., Juan, J.M., Sanz, J.: Improvement of global ionospheric VTEC maps by using kriging interpolation technique. J. Atmos. Sol. Terr. Phys. 2005, 67, 1598–1609, 2005	420 421
Rabah M., Z. Zeedan, E. Ghanem, A. Awad and A. Sherif: "Study the feasibility of using PPP for establishing CORS network". Arab J Geosci (2016) 9:613, DOI 10.1007/s12517-016-2647-8, 2016.	422 423
Rovira-Garcia, A., Juan, J.M., Sanz, J., González-Casado, G.: A World-Wide Ionospheric Model for Fast Precise Point Positioning. IEEE Trans. Geosci. Remote Sens. 2015, 53, 4596–4604, 2015.	424 425
Ryan, B.: Single frequency differential positioning using GPS carrier phase observations for stationary receivers, Master of Science dissertation. Retrieved from university of Florida, department of geomatics engineering, 2015.	426 427 428
Sedeek A. A., Doma M. I., Rabah M. and Hamama M. A.: Determination of Zero Difference GPS Differential Code Biases for Satellites and Prominent Receiver Types, Arabian journal of geosciences, vol. 10, January 2017.	429 430 431
Schaer, S.: Mapping and Predicting the Earth's Ionosphere Using the Global Positioning System. Ph.D. Thesis, Astronomical Institute, University of Berne, Bern, Switzerland, 1999.	432 433



Tawfeek H., A. Sedeeq, M. Rabah and G. El-Fiky: “Regional Ionosphere Mapping Using Zero Difference GPS Carrier Phase”. Paper under publishing in Journal of Applied Geodesy, Walter de Gruyter GmbH, 2018.	434 435 436
Zus, F.; Deng, Z.; Heise, S.; Wickert, J.: Ionospheric mapping functions based on electron density fields. GPS Solut. 2017, 21, 873–885, 2017.	437 438 439 440 441